Total electron content in the Mars ionosphere: Temporal studies and dependence on solar EUV flux

Robert J. Lillis,[1] David A. Brain,[1] Scott L. England,[1] Paul Withers,[2] Matthew O. Fillingim,[1] and Ali Safaeinili[3,4]

Received 21 May 2010; revised 2 July 2010; accepted 5 August 2010; published 16 November 2010.

[1] Total electron content (TEC) derived from radar signal distortions is a useful tool in probing the ionosphere of Mars. We consider 26 months of data from the subsurface mode of the Mars Express MARSIS instrument and confirm that the TEC dependence on solar zenith angle (SZA) approximately matches Chapman theory. After detrending this dependence, we find no clear trend with Martian season or dust activity but find that disturbed solar and space weather conditions can produce prolonged higher TEC values and that isolated solar energetic particle events are coincident with short-lived increases in TEC of ~10^{15} m^{-2} at all SZAs. We present the first comparison between TEC and directly measured solar EUV flux in the 30.4 nm He-II line. We find that the relationship between TEC and both He-II line irradiance and $F_{10.7}$ solar radio flux (a long-used EUV proxy) can be expressed as power laws with exponents of 0.54 and 0.44, respectively, in approximate agreement with Chapman theory.

Citation: Lillis, R. J., D. A. Brain, S. L. England, P. Withers, M. O. Fillingim, and A. Safaeinili (2010), Total electron content in the Mars ionosphere: Temporal studies and dependence on solar EUV flux, *J. Geophys. Res.*, *115*, A11314, doi:10.1029/2010JA015698.

1. Background

[2] The dayside ionosphere of Mars has been studied by instruments on many spacecraft over the last several decades using three basic techniques. First, single profiles of species-specific measurements were made by the two Viking retarding potential analyzers [*Hanson et al.*, 1977]. Second, altitude profiles of electron density have been derived via radio occultation by 12 different spacecraft [see *Mendillo et al.*, 2006, Table 1], the great majority of these (~5600 profiles) by Mars Global Surveyor (MGS) [*Tyler et al.*, 2001] and Mars Express [e.g., *Patzold et al.*, 2005], which continues to operate. Third, the Mars Advanced Radar for Subsurface and Ionospheric Sounding (MARSIS) on Mars Express has provided more than 10,000 nadir topside electron density profiles [*Gurnett et al.*, 2005] and several million total electron content measurements [*Safaeinili et al.*, 2007], which are the subject of this paper. All of these measurements have contributed to significantly improving our knowledge of the structure of (particularly) the dayside ionosphere, as well as the relationship between its variability and external drivers such as the solar cycle and solar rotation [*Breus et al.*, 2004; *Withers and Mendillo*, 2005], solar flares [*Mendillo et al.*, 2006], cosmic rays [*Molina-Cuberos et al.*, 2001; *Haider et al.*, 2007], gamma ray bursts [*Espley et al.*, 2008], and solar energetic particle (SEP) events [*Morgan et al.*, 2006; *Espley et al.*, 2007] and internal factors such as neutral density variations [*Bougher et al.*, 2001], crustal magnetic fields, and local plasma processes [*Withers et al.*, 2005; *Duru et al.*, 2006; *Nielsen et al.*, 2007]. We refer the interested reader to *Withers* [2009], which provides a comprehensive review of the basic theoretical background on and observations to date of the Martian dayside ionosphere.

2. The MARSIS Total Electron Content Data Set

[3] The MARSIS experiment on the Mars Express spacecraft consists of two separate investigations. The Active Ionospheric Sounding (AIS) mode operates as a topside ionospheric sounder [*Gurnett et al.*, 2005]. It measures the time delay of radar waves reflected from the ionosphere as a function of radar frequency between 0.1 and 5.5 MHz, allowing for the retrieval of electron density profiles as a function of altitude at altitudes above the ionospheric peak [*Gurnett et al.*, 2005, 2008]. The subsurface (SS) mode operates as a ground-penetrating radar whose primary purpose is to map geologic interfaces and varied materials in the Martian subsurface, including water ice or liquid deposits [*Picardi et al.*, 2005]. It operates between 1.3 and 5.5 MHz, at which frequencies the MARSIS radar echoes are distorted when traversing the ionosphere. This is manifested as a frequency-dependent phase distortion in the radar signal, which depends upon the total electron content (TEC) and integrals of higher-order moments of the electron density profile [*Safaeinili et al.*, 2007]. These distortions provide information

[1] Space Sciences Laboratory, University of California, Berkeley, California, USA.
[2] Center for Space Physics, Boston University, Boston, Massachusetts, USA.
[3] Jet Propulsion Laboratory, Pasadena, California, USA.
[4] Deceased 29 July 2009.

0148-0227/10/2010JA015698

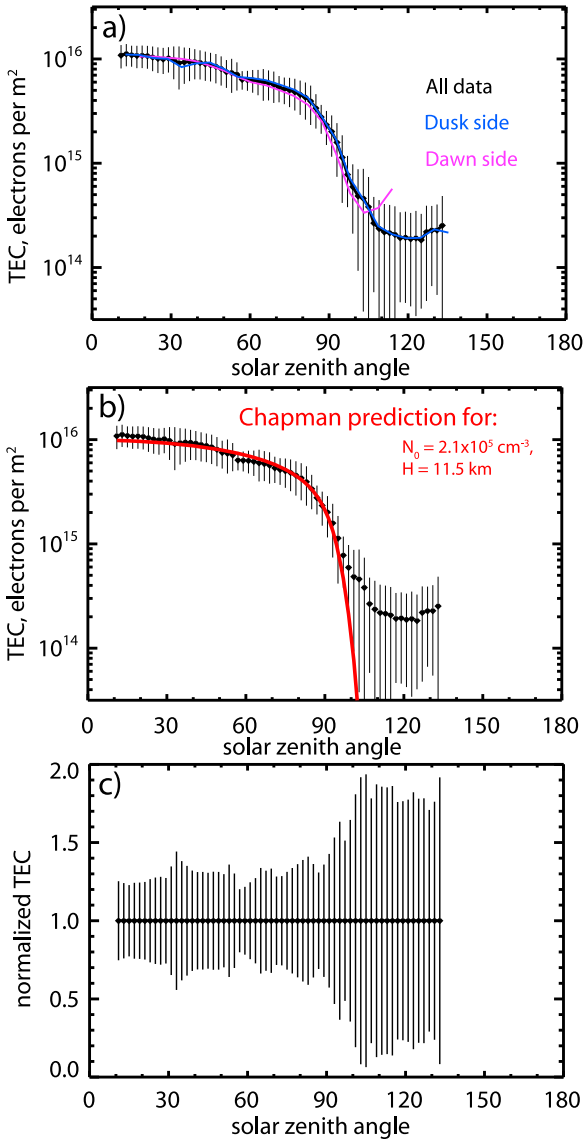

Figure 1. Total electron content (TEC) is binned into 2° bins and plotted as a function of solar zenith angle (SZA) with standard deviations. (a) Overlays the same curve separately for dawn and dusk side. (b) Overlays a Chapman model calculation made with the parameter values printed on the plot. (c) The normalized TEC data set with no solar zenith angle as expected.

on the scale height of the neutral atmosphere H and the subsolar peak electron density N_0, as long as the Chapman ionospheric model [*Chapman*, 1931a, 1931b] is assumed,

$$N_e(z,H,N_0,\chi) = N_0 \,\mathrm{Exp} \cdot \left[\frac{1}{2}\left(1 - \frac{z-z_0}{H} - \mathrm{ch}\left(\frac{R_M + z_0}{H},\chi\right)\exp\left(-\frac{z-z_0}{H}\right)\right)\right],$$

$$\mathrm{TEC}(H,N_0,\chi) = \int_0^\infty N_e(z,H,N_0,\chi)\mathrm{d}z,$$

where z is the altitude, N_e is the electron density, z_0 is the altitude of the subsolar electron density peak, χ is the solar zenith angle (SZA), R_M is the radius of Mars, and ch is the Chapman grazing incidence function that reduces to sec(χ) for sufficiently small SZA [*Chapman*, 1931a]. The Chapman model has been shown to be a reasonably adequate representation of the Mars dayside ionosphere [*Withers*, 2009]. *Safaeinili et al.* [2007] used the measured dependence of the phase distortion on SZA for each terminator crossing over 750 orbits from June 2005 to September 2006 to estimate H and N_0 for each orbit, reporting that the retrieved neutral scale height was significantly lower at sunrise (~10 km) than sunset (~15 km).

[4] In this paper, we wish to concentrate on a sample of interesting correlative results from the public data set of TEC, spanning 19 June 2005 to 30 September 2007 (ftp://psa.esac.esa.int/pub/mirror/MARS-EXPRESS/MARSIS/) and to demonstrate its usefulness in studying the Martian ionosphere. We take a broad overview of the TEC data set, leaving studies of specific orbits to future work. The primary advantage of this data set is its size, comprising ~1.4 million measurements of total electron content between the spacecraft and the surface, with varying, but generally adequate, coverage with respect to latitude, longitude, local time, Martian season, solar zenith angle, crustal magnetic field strength, and topology (these latter two affect ionization by electron precipitation). The primary disadvantage of this TEC data set is that it contains no information about the vertical structure of the ionosphere. Examination of typical electron density profiles from the MGS radio occultation experiment [*Tyler et al.*, 2001] shows that plasma between 100 and 200 km, an altitude range that encompasses the main layers of the ionosphere, is responsible for more than 90% of the total electron content of the ionosphere. Hence, variations in TEC are primarily sensitive to variations in ionospheric density at these altitudes and are relatively insensitive to even large fractional changes in the higher-altitude (>200 km) topside ionosphere.

3. Solar Zenith Angle Dependence of TEC

[5] The strongest dependence of TEC is on solar zenith angle and this dependence follows Chapman theory quite closely, as shown previously for individual orbits [*Safaeinili et al.*, 2007; *Mouginot et al.*, 2008]. Figure 1a shows this relationship for the entire data set in 2° bins of SZA. Relative standard deviations are substantially larger for the nightside due to a combination of larger intrinsic variations in the nightside ionosphere (as reported by *Gurnett et al.* [2008]) and also larger fractional uncertainties in TEC estimations due to a fairly constant absolute uncertainty in the retrieval technique (discussion of this uncertainty can be found in the work of *Mouginot et al.* [2008]). Separate curves for dawn and dusk sides of the planet are also shown. Dawn TEC appears consistently 5%–25% lower for 60° < SZA <100° while somewhat larger for more nightward solar zenith angles where dawn sampling is very sparse. A Chapman curve is shown in Figure 1b for the mean values of N_0 (2.1×10^{11} m^{-3}) and H (11.5 km) derived by *Safaeinili et al.* [2007], providing a reasonable match to the entire TEC data set for SZA < 95°, as expected given this earlier work (note that this comparison is merely a confirmation of earlier work with a larger data set and thus we did not attempt an independent fit, which would require the higher-order moments and a much more detailed analysis of the phase distortion beyond the scope of this paper).

[6] However, for our purposes, we wish to remove this dependence so that we may examine correlations between TEC and other factors, such as EUV flux. To that end, we produced an associated data set of dimensionless "normalized TEC" by separating the TEC values into bins of 2° in SZA, calculating the mean TEC in each bin and dividing all TEC measurements within that bin by the mean. Normalized TEC as a function of SZA, binned in the same fashion, must therefore be equal to unity for all solar zenith angles, as shown along with standard deviations in Figure 1c.

4. Temporal Variations in TEC; Correlations With Solar Activity

[7] The sampling is uneven with respect to Mars solar longitude (Ls) with some substantial gaps. Figures 2a, 2b, and 2d show how normalized TEC and TEC versus SZA curves vary with respect to Ls (with the zero point chosen as the start of Mars year 28 or 21 January 2006/1300:00 UT). Because solar energetic particles have been shown to cause ionospheric disturbances at Mars [*Morgan et al.*, 2006; *Espley et al.*, 2007], we concurrently plot the solar energetic particle (SEP) proxies derived by summing all counts from the energy channels above 10 keV from the electron spectrometers on both Mars Global Surveyor [*Mitchell et al.*, 2001] and Mars Express [*Barabash et al.*, 2004] (Figure 2c). In this energy range, most of the recorded counts are due to >20 MeV protons penetrating the instrument housing and interacting with the microchannel plates (details can be found in the work of *Brain et al.* [2010]).

[8] Solar flare X-ray photons have been shown to cause substantial ionization in the Martian atmosphere [*Mendillo et al.*, 2006], so we also concurrently plot the 0.1–0.8 nm X-ray flux measured by the GOES 12 satellite in Earth orbit in Figure 2e, along with the Earth-Mars angular separation in order to judge how these flares may have impacted Mars. In addition, 1 day averages are plotted (in Figure 2f) of the irradiance in a narrow band surrounding the 30.4 nm Helium-II solar EUV line, as measured by the TIMED-SEE instrument [*Woods and Eparvier*, 2006] in Earth orbit, then scaled appropriately and time-shifted for Mars' position with respect to Earth, assuming a solar rotation period of 27 days. This EUV line is the dominant producer of photoelectrons in the Martian atmosphere via seven branches of photoionization of the two main neutral constituents, atomic oxygen [*Mantas and Hanson*, 1979], and carbon dioxide [*Padial et al.*, 1981].

[9] Finally, since dust storms can substantially affect the neutral thermosphere and hence the ionosphere, 10 day averages of dust opacity from the THEMIS instrument [*Smith*, 2009] are also plotted for comparison in Figure 2f.

[10] With the exception of the disturbed interval prior to Ls = -100° (to be discussed later), normalized TEC is quite constant (within errors) with respect to season, for SZA <80°, as shown by the black, pink, and blue curves in Figure 2b. As SZA increases beyond 80°, we see progressively more variation. For example, the SZA = 80°–90° (green) curve increases by ~15% between Ls = 165° and 185° before falling after perihelion at Ls = 250°. For solar zenith angles greater than 90° (red, purple, and orange curves), we see substantially more variability as the following occur: constant absolute uncertainties account for a larger fraction of the total TEC, the influence of solar photons decreases, and the influence of more variable factors (plasma transport, precipitating protons, and electrons) increases. Overall, despite an apparent tendency for somewhat lower TEC values near the equinoxes and away from the solstices (i.e., near Ls = ~0° and ~140°), it is difficult to discern a clear correlation between TEC and Martian season.

[11] There are several interesting periods of elevated TEC in Figures 2b and 2d. The largest occurs around perihelion of Mars year 27, with three distinct increases, covering at least the interval between Ls = −124° and −94° (25 June to 10 August 2005). Data coverage precludes identification of a beginning or end to this period of disturbed, elevated TEC. It is especially noteworthy because substantial fractional increases in TEC are seen at all SZA where data exist (factors of 3–5), as shown in Figures 2a, 2b, and 2d and Figures 3a and 3c (which shows this increase in more detail). We can see that there was little dust activity in the lower Martian atmosphere at the time. There was however substantial solar activity, which persisted from June until September 2005 (Ls = −130° to −80°) [*Caroubalos et al.*, 2009], in localized active regions on the sun, which rotated in and out of view of the Earth-based instruments recording solar X-rays and solar EUV (i.e., solar rotation caused the modulations apparent in Figures 2e and 2f) and the MGS MAG/ER and Mars Express ELS instruments measuring SEP flux proxies [*Brain et al.*, 2010].

[12] Though Earth and Mars were separated by a relatively small angular distance (30°–45°) during this time, the longevity of these solar disturbances (coupled with solar rotation) implies that significant ionization effects on the Martian atmosphere during this time would be likely, regardless of the separation. The disturbances modulated the EUV flux by ~30% and caused more than a dozen large flares observed at Earth during this time, three of which reached X-class [*Caroubalos et al.*, 2009]. In addition, three separate SEP events occurred at Mars between Ls = −111° and −95°, including a likely coronal mass ejection (CME) shock "spike" signature at Ls = −105° (such "spikes" in energetic particle fluxes during SEP events are signatures of accelerated plasma and in this case the spike was associated with a moderate increase in magnetic field magnitude, both common features of CME shocks [e.g., *Smith and Phillips*, 1997; *Reames et al.*, 1996]), which were related to those active regions. Such disturbed solar conditions should lead to increased TEC from photoionization from the active regions themselves, in addition to ionization from both electrons precipitating in regions of open magnetic field lines [e.g., *Lillis et al.*, 2009] and energetic protons, with their much larger gyroradii, precipitating all over the planet [e.g., *Leblanc et al.*, 2002].

[13] There are also some very abrupt "spikes" in TEC lasting on the order of 1–4 (Earth) days, such as those seen at Ls = 131.0° (7 November 2006) and 146.5° (7 December 2006). These "spikes" are in fact approximately similar absolute increases in TEC at all SZA for which data exist and show up as larger increases in normalized TEC at higher SZA because of the much lower baseline TEC for SZA > 90°. We plot the TEC versus SZA curves for both of these increases in Figure 2a and show a detailed temporal picture in Figures 3f–3j. Unfortunately, the data coverage only allows us to see a fraction of the Ls = 131 event. Again, there is no dust activity to speak of (in any event, these increases are too sudden to be plausibly triggered by dust storm activity). This is also a time of low EUV flux. There is

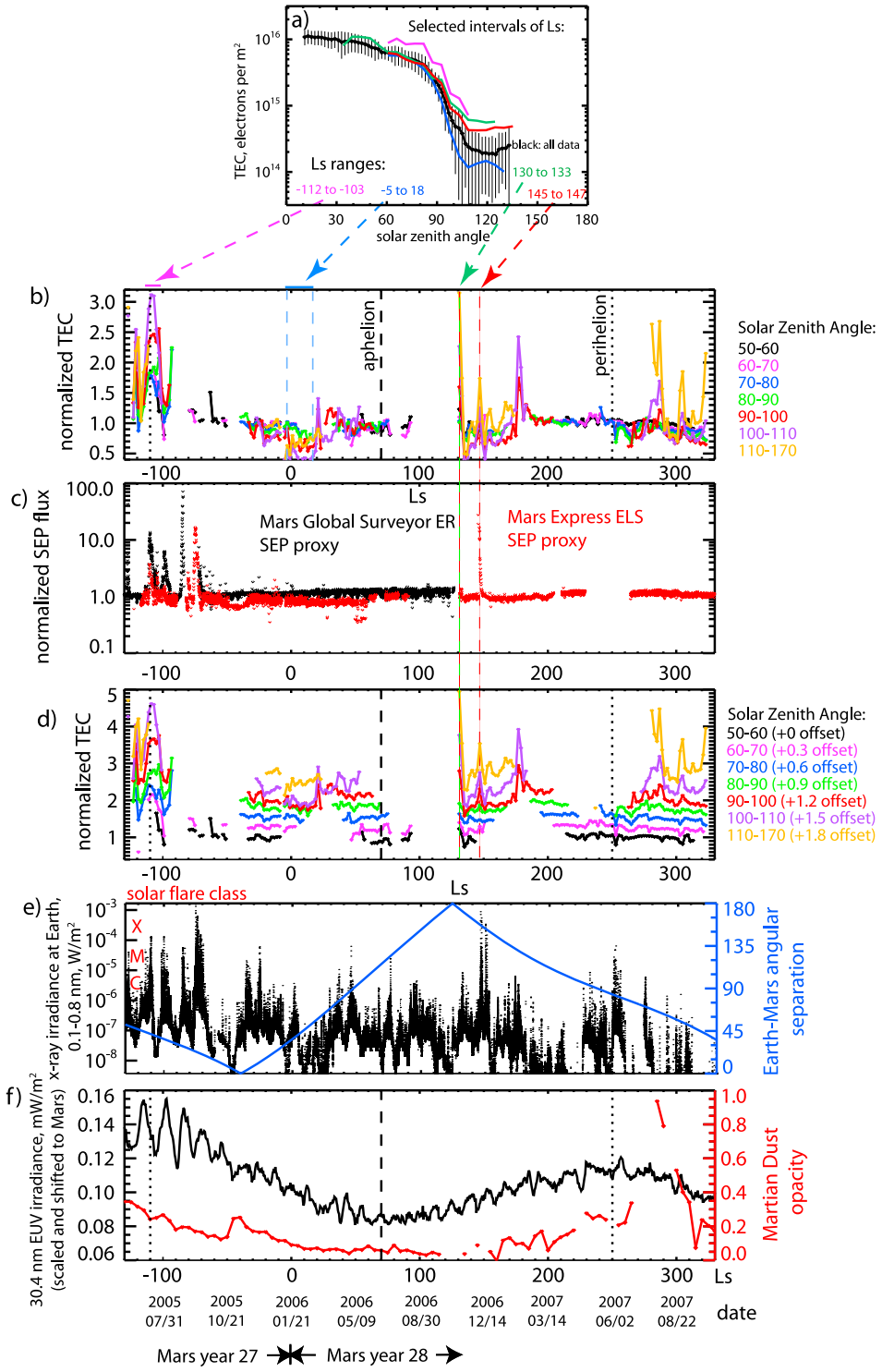

Figure 2. Overview of TEC data set (June 2005 to September 2007). (a) Plots TEC from all data as a function of SZA (as in Figure 1a) and overlays TEC curves corresponding to four periods of interest, identified by colored arrows. (b–f) Time series plots as a function of date and Mars solar longitude (Ls) with respect to Mars year 28. (b) Normalized TEC in different ranges of solar zenith angle. (c) Normalized proxies for solar energetic particle flux (see text). (d) Identical to panel Figure 2b, but with the curves offset for clarity. (e) Simultaneously plots 0.1–0.8 nm solar X-ray irradiance from the Earth-orbiting GOES 12 satellite and the Earth-Mars angular separation. (f) Simultaneously plots solar EUV irradiance in the 30.4 nm He-II line as measured by the TIMED-SEE instrument (scaled and phase-shifted from Earth to Mars) and globally averaged Martian dust opacity as measured by the THEMIS instrument (the discontinuous line results from data gaps).

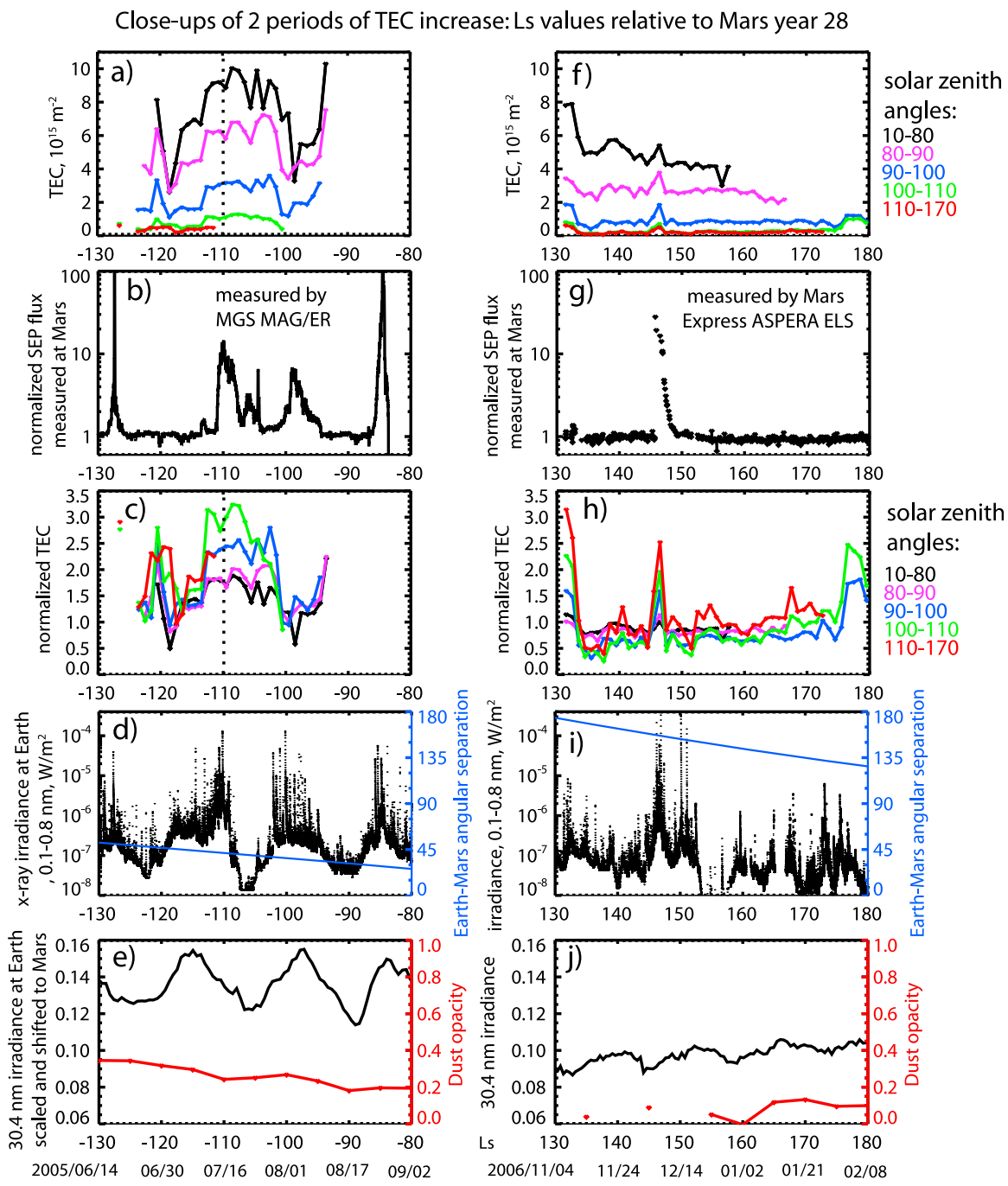

Figure 3. Close-ups of two periods of TEC increase. The Ls values are relative to Mars year 28. Vertically, the two columns show the same quantities as Figures 2b–2f with the exception that Figures 3a and 3f plot absolute TEC instead of normalized TEC to more clearly show absolute increases at different solar zenith angles.

however a single, strong SEP event correlated exactly in time with the latter increase at Ls = 146.5° [*Futaana et al.*, 2008]. The SEP proxy increases by a factor of 30 and the TEC increases by ~1.3×10^{15} m^{-2} for SZA < 100° and by ~0.7×10^{15} m^{-2} for SZA > 100°. The increase at Ls = 131° is larger; however; there is no detectable associated SEP event, although there is a short gap in the SEP proxy coverage at almost exactly this time between Ls = 128° and 130° (green vertical line in Figure 2c), so it is possible that a short, sharp event could have occurred and was not detected. However, there are also substantial increases in TEC, at least for SZA > 90° at Ls = 288° and 305° with no significant EUV increases or SEP events. There was higher dust activity around this time, but the peak in dust opacity appears much broader (despite data gaps) than either of the peaks in TEC, weakening the case for a causal connection, though one cannot be entirely ruled out. This major increase in TEC remains enigmatic.

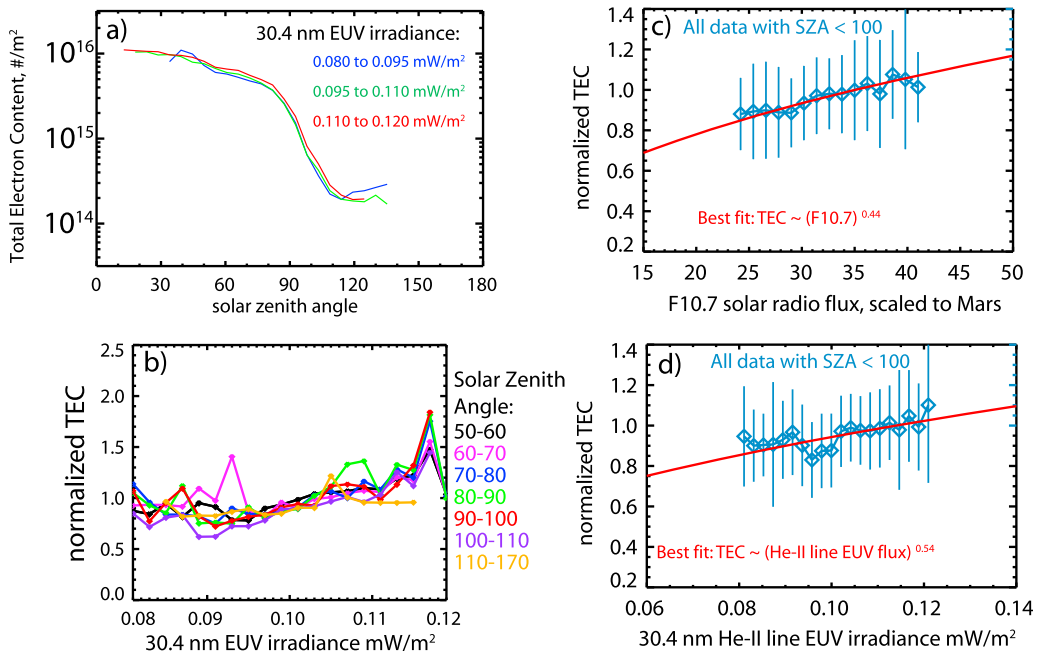

Figure 4. Examination of EUV dependence of TEC. (a) TEC as a function of SZA for three different ranges of 30.4 nm EUV irradiance. (b) Normalized TEC as a function of 30.4 nm irradiance for seven different ranges of SZA. (c and d) Normalized TEC as a function of $F_{10.7}$ solar radio flux (EUV proxy) and directly measured 30.4 nm EUV irradiance for all data with SZA < 100°, respectively, both scaled and shifted from Earth to Mars. Best-fit power laws are drawn through each.

[14] Overall, the observational evidence confirms, with a more quantitative data set, the findings of *Morgan et al.* [2006] and *Espley et al.* [2007], that solar energetic particles impacting neutrals cause substantial ionization, but that a rich variety of processes is likely required to explain all TEC variability in the Martian atmosphere.

5. Correlating TEC With Solar EUV Flux

[15] We also wish to examine the general relationship between TEC and EUV flux at Mars. The TEC data set spans 30.4 nm irradiances between 0.08 and 0.16 W/m^2 (Figure 2f). However, all of the TEC data collected when the irradiance was above 0.12 W/m^2 was during the disturbed period between Ls = −125° and −95°, when not only did several SEP events occur and a CME shock pass the planet but the solar wind pressure (as deduced from MGS magnetometer data) was both strong and highly variable (data not shown). Therefore, we choose to exclude this "disturbed" data when examining the relationship between EUV flux and TEC. Figure 4 demonstrates this relationship for values of 30.4 nm EUV irradiance between 0.08 and 0.12 W/m^2. Figures 4a and 4b show a clearly positive trend for SZA < ~105°.

[16] Chapman theory [*Chapman*, 1931a, 1931b] states that, for a monoenergetic photon flux, the ionization rate is proportional to the intensity, while the equilibrium electron density is proportional to the square root of the ionization rate. Therefore, in this idealized scenario, normalized TEC should vary as the square root of the EUV flux for all sunlit solar zenith angles. A number of past studies have used the $F_{10.7}$ solar radio flux as a proxy for EUV flux and have attempted to fit for the exponent k in the expression relating it to the subsolar peak electron density: $N_0 \propto F_{10.7}^k$. Those using radio occultation profiles have derived values between 0.24 and 0.37 [*Withers*, 2009], while *Morgan et al.* [2006] used MARSIS AIS mode data to derive an exponent of 0.44. As shown in Figure 4c, we also find that normalized TEC (which is directly proportional to subsolar peak density in Chapman theory), for all SZA < 100, varies as a power law with $F_{10.7}$ with an exponent equal to 0.44 ± 0.01.

[17] It can be argued that the $F_{10.7}$ proxy is no longer necessary to use since direct EUV measurements now exist from the TIMED-SEE instrument. Therefore, we also compare TEC with the aforementioned directly measured 30.4 nm irradiance, as shown in Figure 4d. We find the best fit power law exponent to be 0.54 ± 0.01, close to the Chapman-predicted value of 0.5. It is difficult to draw any firm conclusions from this similarity because we cannot easily separate true departure from Chapman theory from uncertainties associated with phase shifting the 30.4 nm measurements from Earth to Mars. However, it does suggest that Chapman theory may provide an adequate representation of vertically integrated electron density at Mars.

6. Conclusions

[18] In this paper, we have shown that the recently released (February 2010) data set of total electron content from the MARSIS Subsurface Sounding mode can be a useful tool in probing the ionosphere of Mars. We have confirmed the initial results of *Safaeinili et al.* [2007] that the dayside TEC data matches the Chapman theory dependence on SZA quite closely. We have removed (insofar as possible) the dependence of TEC on solar zenith angle in order to examine other

correlations. We have examined the temporal behavior of TEC and found that, while there is a slight tendency for lower TEC values near equinox compared to solstice, there is no clear seasonal trend. We have found that disturbed solar and space weather conditions at Mars may produce prolonged higher TEC values and that individual solar energetic particle events may cause a short-lived absolute increase in TEC at all SZAs of $\sim 10^{15}$ m^{-2}. Other temporal increases in TEC have no obvious causes, though atmospheric dust activity cannot be entirely ruled out. Finally, we presented the first comparison between Martian ionospheric properties and directly measured solar EUV flux in the important 30.4 nm He-II line. We find that the relationship between TEC and both He-II line irradiance and $F_{10.7}$ solar radio flux can be expressed as power laws with exponents of 0.54 and 0.44, respectively.

[19] This is only a small sample of the possible investigations that could be carried out with this useful data set. Particularly on the night side, patterns of ionization should be strongly dependent on geographic location and local time as the planet-fixed crustal magnetic fields connect and reconnect with the draped magnetotail field, forming a dynamic system of open and closed magnetic field lines that permits and denies superthermal electrons access to the collisional atmosphere where they cause ionization [*Fillingim et al.*, 2007; *Lillis et al.*, 2009]. This system should vary with solar wind pressure and interplanetary magnetic field (IMF) direction. In addition, more detailed temporal studies should be carried out with respect to individual solar flares and solar energetic particle events.

[20] **Acknowledgments.** This paper is dedicated to the memory of Ali Safaeinili (1961–2009), a dear colleague and excellent scientist. We would like to thank Ali's wife Lisa Safaeinili for her kind permission to put Ali's name on this paper, as he was very much involved in the planning stages of this collaboration. We would like to thank the MARSIS team in Grenoble, France (J. Mouginot and W. Kofman) for producing this very useful data set, as well as the ASPERA-3 team, without whom the SEP flux proxy would not be possible past November 2006 (when MGS was lost). We would also like to thank Amir Caspi for help in plotting the GOES X-ray data, Michael Smith for providing the THEMIS dust opacity data, Philip Chamberlin for help in accessing the TIMED-SEE data, and lastly the European Space Agency's Planetary Science Archive for kindly archiving the TEC data set. This work was supported by NASA Mars Fundamental Research Program grant NNX09AD43G and NASA Mars Data Analysis Program grant NNX08AK94G. R. J. Lillis thanks Stas Barabash and Eduard Dubinin for their assistance in evaluating and improving this paper.

[21] Philippa Browning thanks Stas Barabash and Eduard Dubinin for their assistance in evaluating this paper.

References

Barabash, S., et al. (2004), The Analyzer of Space Plasmas and Energetic Atoms (ASPERA-3) for the European Mars Express mission, *ESA Spec. Publ., SP-1240*, 121–139.

Bougher, S. W., S. Engel, D. P. Hinson, and J. M. Forbes (2001), Mars Global Surveyor Radio Science electron density profiles: Neutral atmosphere implications, *Geophys. Res. Lett.*, *28*, 3091–3094.

Brain, D. A., G. T. Delory, R. J. Lillis, D. Ulusen, D. Mitchell, and J. Luhmann (2010), Mars Global Surveyor measurements of solar storms and their effects, in *Radiation Effects From the Sun to Mars*, edited by S. McKenna-Lawlor, IAAA, in press.

Breus, T. K., A. M. Krymskii, D. H. Crider, N. F. Ness, D. Hinson, and K. K. Barashyan (2004), Effect of the solar radiation in the topside atmosphere/ionosphere of Mars: Mars Global Surveyor observations, *J. Geophys. Res.*, *109*, A09310, doi:10.1029/2004JA010431.

Caroubalos, C., P. Preka-Papadema, H. Mavromichalaki, X. Moussas, A. Papaioannou, E. Mitsakou, and A. Hillaris (2009), Space storm measurements of the July 2005 solar extreme events from the low corona to the Earth, *Adv. Space Res.*, *43*(4), 600–604, doi:10.1016/j.asr.2008.09.019

Chapman, S. (1931a), The absorption and dissociative or ionizing effect of monochromatic radiation in an atmosphere on a rotating Earth, *Proc. Phys. Soc. London*, *43*, 26– 45.

Chapman, S. (1931b), The absorption and dissociative or ionizing effect of monochromatic radiation in an atmosphere on a rotating Earth: Part II. Grazing incidence, *Proc. Phys. Soc. London*, *43*, 483– 501.

Duru, F., D. A. Gurnett, T. F. Averkamp, D. L. Kirchner, R. L. Huff, A. M. Persoon, J. J. Plaut, and G. Picardi (2006), Magnetically controlled structures in the ionosphere of Mars, *J. Geophys. Res.*, *111*, A12204, doi:10.1029/2006JA011975.

Espley, J. R., W. M. Farrell, D. A. Brain, D. D. Morgan, B. Cantor, J. J. Plaut, M. H. Acuña, and G. Picardi (2007), Absorption of MARSIS radar signals: Solar energetic particles and the daytime ionosphere, *Geophys. Res. Lett.*, *34*, L09101, doi:10.1029/2006GL028829.

Espley, J. R., J. E. C. Connerney, and R. J. Lillis (2008), Effects of high energy astrophysical events on the Martian Atmosphere, in Third International Workshop on the Mars Atmosphere: Modeling and Observations, *Lunar and Planet. Inst.*, Williamsburg, Va., 8–13 Nov.

Fillingim, M. O., L. M. Peticolas, R. J. Lillis, D. A. Brain, J. S. Halekas, D. L. Mitchell, R. P. Lin, D. Lummerzheim, S. W. Bougher, and D. L. Kirchner (2007), Model calculations of electron precipitation induced ionization patches on the nightside of Mars, *Geophys. Res. Lett.*, *34*, L12101, doi:10.1029/2007GL029986.

Futaana, Y., et al. (2008), Mars Express and Venus Express multipoint observations of geoeffective solar flare events in December 2006, *Planet. Space Sci.*, *56*, 873–880.

Gurnett, D. A., et al. (2005), Radar soundings of the ionosphere of Mars, *Science*, *310*(5756), 1929–1933, doi:10.1126/science.1121868.

Gurnett, D. A., et al. (2008), An overview of radar soundings of the Martian ionosphere from the Mars Express spacecraft, *Adv. Space Res.*, *41*, 1335–1346.

Haider, S. A., V. Singh, V. R. Choksi, W. C. Maguire, and M. I. Verigin (2007), Calculated densities of H_3O^+ $(H_2O)_n$, NO_2^- $(H_2O)_n$, CO_3^- $(H_2O)_n$ and electron in the nighttime ionosphere of Mars: Impact of solar wind electron and galactic cosmic rays, *J. Geophys. Res.*, *112*, A12309, doi:10.1029/2007JA012530.

Hanson, W. B., S. Sanatani, and D. R. Zuccaro (1977), The Martian ionosphere as observed by the Viking retarding potential analyzers, *J. Geophys. Res.*, *82*, 4351–4363, doi:10.1029/JS082i028p04351.

Leblanc, F., J. G. Luhmann, R. E. Johnson, and E. Chassefiere (2002), Some expected impacts of a solar energetic particle event at Mars, *J. Geophys. Res.*, *107*(A5), 1058, doi:10.1029/2001JA900178.

Lillis, R. J., M. O. Fillingim, L. M. Peticolas, D. A. Brain, R. P. Lin, and S. W. Bougher (2009), The nightside ionosphere of Mars: Modeling the effects of crustal magnetic fields and electron pitch angle distributions on electron impact ionization, *J. Geophys. Res.*, *114*, E11009, doi:10.1029/2009JE003379.

Mantas, G. P., and W. B. Hanson (1979), Photoelectron fluxes in the Martian ionosphere, *J. Geophys. Res.*, *84*(A2), 369–385, doi:10.1029/JA084iA02p00369.

Mendillo, M., P. Withers, D. Hinson, H. Rishbeth, and B. Reinisch (2006), Effects of solar flares on the ionosphere of Mars, *Science*, *311*, 1135–1138.

Mitchell, D. L., R. P. Lin, C. Mazelle, H. Reme, P. A. Cloutier, J. E. P. Connerney, M. H. Acuña, and N. F. Ness (2001), Probing Mars' crustal magnetic field and ionosphere with the MGS Electron Reflectometer, *J. Geophys. Res.*, *106*(E10), 23,419, doi:10.1029/2000JE001435.

Molina-Cuberos, G. J., J. J. Lopez-Moreno, R. Rodrigo, H. Lichtenegger, and K. Schwingenschuh (2001), A model of the Martian ionosphere below 70 km, *Adv. Space Res.*, *27*, 1801–1806.

Morgan, D. D., D. A. Gurnett, D. L. Kirchner, R. L. Huff, D. A. Brain, W. V. Boynton, M. H. Acuña, J. J. Plaut, and G. Picardi (2006), Solar control of radar wave absorption by the Martian ionosphere, *Geophys. Res. Lett.*, *33*, L13202, doi:10.1029/2006GL026637.

Mouginot, J., W. Kofman, A. Safaeinili, and A. Herique (2008), Correction of the ionospheric distortion on the MARSIS surface sounding echoes, *Planet. Space Sci.*, *56*, 917–926.

Nielsen, E., et al. (2007), Local plasma processes and enhanced electron densities in the lower ionosphere in magnetic cusp regions on Mars, *Planet. Space Sci.*, *55*, 2164–2172.

Padial, N., G. Csanak, B. V. McKoy, and P. W. Langhoff (1981), Photoexcitation and ionization in carbon dioxide: Theoretical studies in the separated-channel static-exchange approximation, *Phys. Rev. A*, *23*, 218–235.

Patzold, M., S. Tellmann, B. Hausler, D. Hinson, R. Schaa, and G. L. Tyler (2005), A Sporadic third layer in the ionosphere of Mars, *Science*, *310*, 837–839.

Picardi, G., et al. (2005), Radar soundings of the subsurface of Mars, *Science*, *310*(5756), 1925–1928, doi:10.1126/science.1122165.

Reames, D. V., L. M. Barbier, and C. K. Ng (1996), The spatial distribution of particles accelerated by coronal mass ejection-driven shocks, *Astrophys. J.*, *466*, 473–486, doi:10.1086/177525.

Safaeinili, A., W. Kofman, J. Mouginot, Y. Gim, A. Herique, A. B. Ivanov, J. J. Plaut, and G. Picardi (2007), Estimation of the total electron content of the Martian ionosphere using radar sounder surface echoes, *Geophys. Res. Lett.*, *34*, L23204, doi:10.1029/2007GL032154.

Smith, C. W., and J. L. Phillips (1997), The role of coronal mass ejections and interplanetary shocks in interplanetary magnetic field statistics and solar magnetic flux ejection, *J. Geophys. Res.*, *102*(A1), 249–261, doi:10.1029/96JA02678.

Smith, M. D. (2009), THEMIS Observations of Mars Aerosol Optical Depth from 2002–2008, *Icarus*, *202*, 444–452.

Tyler, G. L., G. Balmino, D. P. Hinson, W. L. Sjogren, D. E. Smith, R. A. Simpson, S. W. Asmar, P. Priest, and J. D. Twicken (2001), Radio science observations with Mars Global Surveyor: Orbit insertion through one Mars year in mapping orbit, *J. Geophys. Res.*, *106*(E10), 23,327–23,348, doi:10.1029/2000JE001348.

Withers, P. (2009), A review of variability in the dayside ionosphere of Mars, *Adv. Space Res.*, *44*(3), 277–307.

Withers, P., and M. Mendillo (2005), Response of peak electron densities in the Martian ionosphere to day-to-day changes in solar flux due to solar rotation, *Planet. Space Sci.*, *53*, 1401–1418.

Withers, P., M. Mendillo, H. Rishbeth, D. P. Hinson, and A. J. Arkani-Hamed (2005), Ionospheric characteristics above Martian crustal magnetic anomalies, *Geophys. Res. Lett.*, *32*, L16204, doi:10.1029/2005GL023483.

Woods, T. N., and F. G. Eparvier (2006), Solar ultraviolet variability during the TIMED mission, *Adv. Space Res.*, *37*, 219–224.

D. A. Brain, S. L. England, M. O. Fillingim, and R. J. Lillis, Space Sciences Laboratory, University of California, 7 Gauss Way, Berkeley, CA 94720, USA. (rlillis@ssl.berkeley.edu)

P. Withers, Center for Space Physics, Boston University, 725 Commonwealth Ave., Boston, MA 02215 USA.